

Crystallinity effects on the surface optical response in metals: A preliminary calculation

J. T. Lee and W. L. Schaich

Department of Physics and Institute for Materials Research, Indiana University, Bloomington, Indiana 47405

(Received 28 September 1990)

The beginning of a practical evaluation scheme for dynamic screening at the surface of a crystalline metal is developed. The derivation shows how band-structure effects on the d parameters may be calculated. Simplified versions of the basic equations are evaluated for a model of the (110) face of Li. Several features, absent from jellium models, are shown to make significant contributions. The theory is still too approximate for direct comparisons with experiment, but indicates a feasible path towards that goal.

I. INTRODUCTION

For some time there has been a strong interest in and a considerable effort expended on the surface optical response of metals. Even a list of review articles on this subject is rather long.¹⁻¹¹ However, at least for metals at the microscopic level of interest here, theoretical work has almost exclusively been devoted to jellium models. Such calculations can now be done with considerable sophistication and relative ease,¹² but they all omit from the outset any microscopic allowance for crystallinity effects. This limitation has recently become a more pressing concern due to the surge in experimental work¹³⁻¹⁸ that can be directly compared with theoretical predictions. Certainly a jellium model of Ag can only hope to be qualitative, and even for the alkali metals or Al it is not obvious that subtle differences in the treatment of many-body effects have more quantitative importance than the inclusion of lattice scattering.

In this paper we begin the development of a theory that will allow tractable estimates of the influence of band structure on surface optical response. Our specific emphasis here will be on understanding the features that can appear far (on the scale of screening lengths) from the surface. In Figs. 1 and 2 we illustrate some of the changes that occur in switching from a jellium to a crystalline substrate. The quantity plotted is the (specially scaled) component of the electric field normal to the surface as a function of depth into the sample. Such curves summarize the mean-field linear response of the system to a long-wavelength external perturbation at a fixed frequency. In Fig. 1 the obvious new feature is the appearance of periodic oscillations tied to the lattice constant. These accompany any field that extends into the bulk and are the "local-field" terms that one suppresses in macroscopic electrodynamics.¹⁹

In a different range of driving frequency additional oscillations with periods larger than the lattice constant can appear in the asymptotic behavior. An example is shown in Fig. 2 where the frequency lies within the band of zone-boundary collective states. The existence of these modes depends on the presence of gaps in the electronic energy spectrum, hence on the deviations of the system from a jellium model. Their influence on electron-

energy-loss spectra has been calculated before²⁰⁻²² and confirmed by experiment. Our theory shows how they appear in the surface optical response.

In the rest of the paper we describe how these and further calculations can be done. Section II contains the basic derivation and introduces the several approximations necessary (at this stage) to obtain tractable formulas. Then in Sec. III we describe the model calculations that we have done, illustrating various theoretical ingredients and consequences. Although our present numerical results only have a qualitative validity, this paper should be a useful theoretical guide to more sophisticated evaluations.

II. FORMALISM

In an abstract sense, the problem of the surface optical response of a crystal has already been solved, in that several general (and essentially equivalent) schemes have

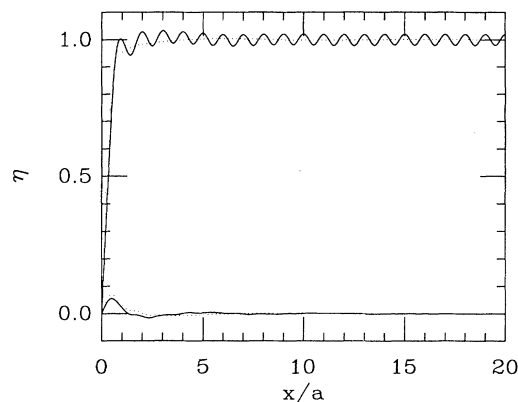


FIG. 1. For a model of the (110) face of crystalline Li subjected to a perturbation at a frequency of $\frac{1}{2}$ the free-electron Fermi energy ϵ_F^0 , we plot the function η from Eq. (32) vs distance into the substrate, with a the interplanar spacing along the surface normal. The solid curves give the real and imaginary parts of η , while the dotted curves are the corresponding jellium results.

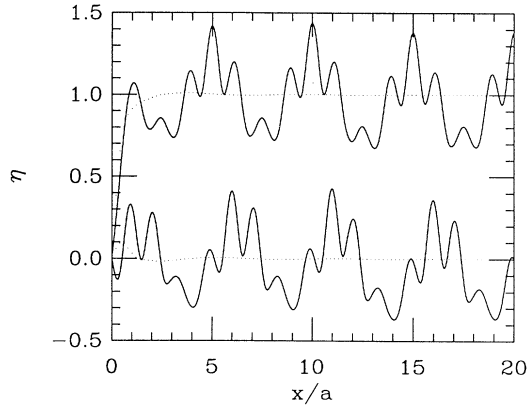


FIG. 2. Same as Fig. 1 except the frequency of the external perturbation is now $0.9\epsilon_p^0$. The two dominant periods in the oscillations are close to $5a$ and $5a/4$ and both are associated with the zone boundary collective state.

been derived.^{23–28} However, there have been few attempts to convert these formal theories into practical results. Most of the numerical work has focused on semiconductors or insulators (see Refs. 29–31 for recent examples) and usually the analysis does not consider p -polarized light. In metals it is this case, or more precisely the response to a normal electric field, that has been of primary interest. So in the language of d -parameter theory, it is d_{\perp} rather than d_{\parallel} that we wish (initially) to study. This limited scope has the advantage that one only needs to consider (scalar) density and not (vector) current response. It has the numerical challenge that its evaluation requires the solution of an integral equation. Our goal is to translate the formal recipes in Ref. 28 (hereafter called SC) into modest changes in the jellium codes of Kempa and Schaich.^{32–34}

A. Basic integral equation

We begin with a generalization of the density response theory in Ref. 32. One seeks the electron density $\delta\rho(\mathbf{x}, t)$

$$\delta\rho(x, \mathbf{Q}) = \int dx' \sum_{\mathbf{G}'} \chi_0(x, x'; \mathbf{Q}, \mathbf{K} + \mathbf{G}') \left[\Gamma_e e^{-Kx'} \delta_{\mathbf{G}', 0} + \int dx'' \frac{2\pi e^2}{|\mathbf{K} + \mathbf{G}'|} e^{-|\mathbf{K} + \mathbf{G}'||x' - x''|} \delta\rho(x'', \mathbf{K} + \mathbf{G}') \right], \quad (6)$$

where

$$\chi_0(x, x'; \mathbf{Q}, \mathbf{Q}') = \frac{1}{A} \int d^2X \int d^2X' e^{-i\mathbf{Q}\cdot\mathbf{X}} \chi_0(\mathbf{x}, \mathbf{x}') e^{i\mathbf{Q}'\cdot\mathbf{X}'} \quad (7)$$

In a jellium model, the integrals in Eq. (7) would reproduce a factor of $\delta(\mathbf{Q} - \mathbf{Q}')$, which in turn would remove the sum on \mathbf{G}' in Eq. (6) and replace \mathbf{Q} and $\mathbf{K} + \mathbf{G}'$ with \mathbf{K} .

Our method of solving Eq. (6) is based on taking cosine Fourier transforms of the x dependence according to the definitions³²

induced at first order by an external potential energy of the form

$$V_{\text{ext}}(\mathbf{x}, t) = \Gamma_e e^{-Kx} e^{i(\mathbf{K}\cdot\mathbf{X} - \omega t)}, \quad (1)$$

where the three-dimensional vector \mathbf{x} has been separated into a component x along the normal to the surface plane and a two-dimensional projection \mathbf{X} into the surface plane. The material lies to the right of $x=0$ and the two-dimensional wave vector \mathbf{K} (of magnitude K) will eventually be set to zero. Since all quantities will be at frequency ω , we stop writing factors of $e^{-i\omega t}$ and leave the dependence on ω implicit.

The density response is found within the time-dependent Hartree approximation [or random-phase approximation (RPA)] by writing

$$\delta\rho(\mathbf{x}) = \int d^3x' \chi_0(\mathbf{x}, \mathbf{x}') [V_{\text{ext}}(\mathbf{x}') + V_{\text{ind}}(\mathbf{x}')], \quad (2)$$

where the induced potential energy is

$$V_{\text{ind}}(\mathbf{x}) = \int d^3x' \frac{e^2}{|\mathbf{x} - \mathbf{x}'|} \delta\rho(\mathbf{x}'). \quad (3)$$

In (2), χ_0 is the independent-particle susceptibility. For our description of a simple crystalline surface the system has a discrete translational symmetry in \mathbf{X} and, once one is several lattice constants into the material, also a discrete translational symmetry in x . The reciprocal lattice of the bulk is described by the vectors $\mathbf{g} = (g, \mathbf{G})$ and we assume the projections of \mathbf{g} along or normal to $\hat{\mathbf{x}}$, the surface normal, can be independently varied. The global translational symmetry in \mathbf{X} implies that the perturbation at \mathbf{K} produces a response at all \mathbf{Q} given by

$$\mathbf{Q} = \mathbf{K} + \mathbf{G}. \quad (4)$$

Using this property of χ_0 plus the (two-dimensional) Fourier transform of the Coulomb potential,

$$\frac{1}{|\mathbf{x}|} = \frac{1}{A} \sum_{\mathbf{Q}} \frac{2\pi}{Q} e^{-Q|x|} e^{i\mathbf{Q}\cdot\mathbf{X}}, \quad (5)$$

where A is the total surface area, we obtain for the Fourier transform of the \mathbf{X} dependence of $\delta\rho$

$$S(q) = \int_0^{\infty} dx \cos qx S(x), \quad (8)$$

$$T(q, q') = \frac{2}{\pi} \int_0^{\infty} dx \cos qx \int_0^{\infty} dx' \cos q'x' T(x, x'). \quad (9)$$

The transform of the Coulomb potential energy $V_c(x, x'; \mathbf{Q}) = (2\pi e^2/Q) e^{-Q|x-x'|}$ is

$$V_c(q, q'; \mathbf{Q}) = v(q, \mathbf{Q}) \delta(q - q') - \gamma(\mathbf{Q}) v(q, \mathbf{Q}) v(q', \mathbf{Q}), \quad (10)$$

where

$$v(q, \mathbf{Q}) = \frac{4\pi e^2}{q^2 + Q^2} \quad (11)$$

and

$$\gamma(\mathbf{Q}) = \frac{Q/\pi}{4\pi e^2}, \quad (12)$$

while the transform of the external potential energy $V_e(x) = \Gamma_e e^{-Qx}$ is

$$V_e(q, \mathbf{Q}) = \gamma_e(\mathbf{Q})v(q, \mathbf{Q}), \quad (13)$$

where

$$\gamma_e(\mathbf{Q}) = \frac{Q\Gamma_e}{4\pi e^2}. \quad (14)$$

Applying these results to Eq. (6) yields

$$\begin{aligned} \delta\rho(q, \mathbf{Q}) = & \int_0^\infty dq' \sum_{\mathbf{G}'} \chi_0(q, q'; \mathbf{Q}, \mathbf{K} + \mathbf{G}') \\ & \times v(q', \mathbf{K} + \mathbf{G}') \delta\rho(q', \mathbf{K} + \mathbf{G}') \\ & + \sum_{\mathbf{G}'} \delta\rho_0(q, \mathbf{Q}, \mathbf{K} + \mathbf{G}') [\delta_{\mathbf{G}', 0} - \lambda(\mathbf{K} + \mathbf{G}')], \end{aligned} \quad (15)$$

where

$$\delta\rho_0(q, \mathbf{Q}, \mathbf{Q}') = \int_0^\infty dq' \chi_0(q, q'; \mathbf{Q}, \mathbf{Q}') v(q', \mathbf{Q}') \gamma_e(\mathbf{Q}') \quad (16)$$

and

$$\lambda(\mathbf{Q}) = \frac{\gamma(\mathbf{Q})}{\gamma_e(\mathbf{Q})} \int_0^\infty dq v(q, \mathbf{Q}) \delta\rho(q, \mathbf{Q}). \quad (17)$$

$$\sum_{\mathbf{G}'} A(q; \mathbf{Q}, \mathbf{K} + \mathbf{G}') D_x(x=0, \mathbf{K} + \mathbf{G}')$$

$$= D_x(x=0, \mathbf{Q}) + \int dq' \sum_{\mathbf{G}'} \chi_0(q, q'; \mathbf{Q}, \mathbf{K} + \mathbf{G}') v(q', \mathbf{K} + \mathbf{G}') \sum_{\mathbf{G}''} A(q'; \mathbf{K} + \mathbf{G}', \mathbf{K} + \mathbf{G}'') D_x(x=0, \mathbf{K} + \mathbf{G}''). \quad (22)$$

This may be further simplified by defining

$$\nu(q, \mathbf{Q}) = \sum_{\mathbf{G}'} A(q; \mathbf{Q}, \mathbf{K} + \mathbf{G}') D_x(x=0, \mathbf{K} + \mathbf{G}') / D_x(x=0, \mathbf{K}), \quad (23)$$

so (22) becomes

$$\nu(q, \mathbf{Q}) = D_x(x=0, \mathbf{Q}) / D_x(x=0, \mathbf{K}) + \sum_{\mathbf{G}'} \int_0^\infty dq' \chi_0(q, q'; \mathbf{Q}, \mathbf{K} + \mathbf{G}') v(q', \mathbf{K} + \mathbf{G}') \nu(q', \mathbf{K} + \mathbf{G}'). \quad (24)$$

Working back through the algebra we have from (21)

$$4\pi e \delta\rho(q, \mathbf{Q}) = \nu(q, \mathbf{Q}) D_x(x=0, \mathbf{K}) - D_x(x=0, \mathbf{Q}). \quad (25)$$

Combining Eqs. (17), (20), and (25) allows one to formally solve for $D_x(x=0, \mathbf{Q})$ or $\lambda(\mathbf{Q})$ in terms of ν . These results can be used to reexpress the "driving" term in (24) for $\mathbf{G} \neq 0$ as

$$\begin{aligned} D_x(x=0, \mathbf{K} + \mathbf{G}) / D_x(x=0, \mathbf{K}) \\ = -2\gamma(\mathbf{K} + \mathbf{G}) \int_0^\infty dq v(q, \mathbf{K} + \mathbf{G}) \nu(q, \mathbf{K} + \mathbf{G}), \end{aligned} \quad (26)$$

The physical interpretation of $\lambda(\mathbf{Q})$ is that it represents a reflection amplitude in the sense that for $x < 0$ (in vacuum)

$$\begin{aligned} \lambda(\mathbf{Q}) \Gamma_e e^{Qx} &= \int_0^\infty dx' V_e(x, x'; \mathbf{Q}) \delta\rho(x', \mathbf{Q}) \\ &= \frac{2\pi e^2}{Q} e^{Qx} \int_0^\infty dx' e^{-Qx'} \delta\rho(x', \mathbf{Q}). \end{aligned} \quad (18)$$

Changing to a q integration and using Eqs. (11)–(14) in Eq. (18) gives Eq. (17). Indeed we can write the potential energy in vacuum as

$$e\Phi(\mathbf{x}) = \Gamma_e e^{i\mathbf{K} \cdot \mathbf{x}} \left[e^{-Kx} + \sum_{\mathbf{G}} \lambda(\mathbf{K} + \mathbf{G}) e^{|\mathbf{K} + \mathbf{G}|x} e^{i\mathbf{G} \cdot \mathbf{x}} \right], \quad (19)$$

so the normal component of the displacement (or electric) field is for $x < 0$,

$$\begin{aligned} eD_x(\mathbf{x}) &= \Gamma_e \sum_{\mathbf{G}} e^{i(\mathbf{K} + \mathbf{G}) \cdot \mathbf{x}} |\mathbf{K} + \mathbf{G}| \\ &\times [\delta_{\mathbf{G}, 0} e^{-Kx} - \lambda(\mathbf{K} + \mathbf{G}) e^{|\mathbf{K} + \mathbf{G}|x}]. \end{aligned} \quad (20)$$

Comparing with Eq. (15) we see that a weighted sum of the $D_x(x=0, \mathbf{K} + \mathbf{G}')$ acts as the driving term for $\delta\rho$. This leads us to write

$$\begin{aligned} \delta\rho(q, \mathbf{Q}) &= \sum_{\mathbf{G}'} [A(q; \mathbf{Q}, \mathbf{K} + \mathbf{G}') - \delta_{\mathbf{G}, \mathbf{G}'}] \\ &\times D_x(x=0, \mathbf{K} + \mathbf{G}') / 4\pi e, \end{aligned} \quad (21)$$

which when substituted in Eq. (15) gives an equation for A in which $\delta\rho_0$ does not appear:

which can be viewed as a modification of the effective χ_0 :

$$\chi_0 \rightarrow \chi_0 - 2\delta_{\mathbf{G}, \mathbf{G}'} (1 - \delta_{\mathbf{G}, 0}) \gamma(\mathbf{K} + \mathbf{G}).$$

One next needs to find a reasonable χ_0 and to solve (24) for $\nu(q, \mathbf{Q})$. To ease the computational effort we will make severe approximations at both of these steps. Since our emphasis is on d_{\perp} , we drop all crystallinity effects in \mathbf{X} ; i.e. the only deviation from the jellium model in the bulk is a periodic variation in x . Momentum parallel to the surface is then conserved through the screening pro-

cess, so (24) simplifies to

$$\nu(q) = 1 + \int_0^\infty dq' \chi_0(q, q') v(q') \nu(q'), \quad (27)$$

where, as done earlier for the frequency ω , we have suppressed all reference to the common parallel wave vector $\mathbf{K} \rightarrow 0$. Equation (27) is identical in form to the jellium result, cf. Eq. (24) in Ref. 32. The different answers for the two models depend on differences in χ_0 .

We remark that a much earlier paper on surface optical response³⁵ also approximated the surface of a three-dimensional crystal as a system with only one direction of discrete translational symmetry. However, they were only concerned with the surface-plasmon dispersion and their direction of periodicity was parallel, rather than perpendicular, to the surface plane.

B. Calculable quantities

To further emphasize the formal similarity with equations of the jellium model, we show how the function ν determines all the quantities of interest. Equation (25) now appears as

$$4\pi e \delta\rho(q) = [\nu(q) - 1] D_x(0), \quad (28)$$

where $D_x(0) = D_x(x=0, \mathbf{K} \rightarrow 0)$. Then inverting the transform,

$$4\pi e \delta\rho(x) = D_x(0) \frac{2}{\pi} \int_0^\infty dq \cos qx [\nu(q) - 1], \quad (29)$$

which describes the distribution of screening charge density inside the metal. The left-hand side of (29) also appears in Poisson's equation

$$4\pi e \delta\rho(x) = \nabla \cdot \mathbf{E}. \quad (30)$$

Since the perturbation is long wavelength (and since we have neglected transverse umklapp processes) we can replace $\nabla \cdot \mathbf{E} \approx \partial E_x / \partial x$ and use (29) and (30) to find

$$\begin{aligned} E_x(x) &= E_x(0) + 4\pi e \int_0^x dx' \delta\rho(x') \\ &= D_x(0) + D_x(0) \frac{2}{\pi} \int_0^\infty dq \frac{\sin qx}{q} [\nu(q) - 1] \\ &= D_x(0) \frac{2}{\pi} \int_0^\infty dq \frac{\sin qx}{q} \nu(q). \end{aligned} \quad (31)$$

To within normalization terms this result describes all the curves shown in Figs. 1 and 2. Indeed the η plotted there is given by

$$\eta(x) = \frac{2}{\pi} \int_0^\infty dq \frac{\sin qx}{q} \left[\frac{\nu(q) - 1}{\nu(0) - 1} \right], \quad (32)$$

which vanishes at $x=0$ and whose value, averaged over a unit cell, tends to one deep in the bulk. It is an artifact of the semiclassical infinite barrier model (SCIB) approximation introduced below that η has a nonzero derivative at $x=0^+$ (see Figs. 1, 2, and 8), which implies an unphysical discontinuity in $\delta\rho$ there. The spatial distribution of the near surface behavior of the response is not well described by the SCIB, but this will be repaired by better theories of $\nu(q)$.³⁶

Finally we reduce the formal prescription of SC for d_\perp .

In the present notation this appears as

$$(1 - 1/\epsilon_\perp^m) d_\perp = \int_{-\infty}^\infty dx [E_x(x) - \bar{E}_x^0(x)] / D_x(0), \quad (33)$$

where

$$\bar{E}_x^0(x) = \bar{\Theta}(x) E_x^>(x) + \bar{\Theta}(-x) E_x^<(x) \quad (34)$$

with

$$\bar{\Theta}(x) = \begin{cases} 0, & x < -a/2 \\ x/a + \frac{1}{2}, & -a/2 < x < a/2 \\ 1, & a/2 < x \end{cases} \quad (35)$$

and close (on the scale of transverse wavelengths) to the surface

$$E_x^<(x) = D_x(0), \quad (36)$$

$$E_x^>(x) = \left[\epsilon_0^{-1}(0,0) + 2 \sum_{n>0} \cos(ng_0x) \epsilon_0^{-1}(n,0) \right] D_x(0). \quad (37)$$

The system in bulk has a lattice constant along $\hat{\mathbf{x}}$ equal to a and we represent the corresponding reciprocal-lattice "vectors" by $g = ng_0$, where n is an integer and $g_0 = 2\pi/a$. We assume that the Hamiltonian in bulk has reflection symmetry about at least one point in the unit cell and choose the origin for x at an integer multiple of a away from such a symmetry point and far enough out in vacuum so that no significant equilibrium or induced charge density exists there. This latter choice makes $E_x \approx E_x^<$ for $x < 0$. The symmetric placement of the origin also simplifies the expansion of the bulk "reference field" $E_x^>$. The ϵ 's that appear there are from the microscopic dielectric function to be analyzed below. Their only property that we need here is

$$\epsilon_0^{-1}(0,0) = 1/\epsilon_\perp^{(m)}, \quad (38)$$

where $\epsilon_\perp^{(m)}$ is the macroscopic dielectric function for fields along $\hat{\mathbf{x}}$. The subscript \perp is necessary in (38) because our neglect of crystallinity effects in \mathbf{X} has made the system optically anisotropic.

We begin the simplification of (33) by expressing it as a primary term plus a remainder:

$$(1 - 1/\epsilon_\perp^{(m)}) d_\perp = \int_0^\infty dx [E_x(x) - E_x^>(x)] / D_x(0) + R. \quad (39)$$

Substituting from (31) and (37) the explicit integral in (39) becomes

$$\begin{aligned} \int_0^\infty dx [E_x(x) - E_x^>(x)] / D_x(0) \\ = \frac{2}{\pi} \int_0^\infty dq \frac{[\nu(q) - 1/\epsilon_\perp^{(m)}]}{q^2}, \end{aligned} \quad (40)$$

where we have used the fact that the cosine terms in (37) integrate to zero and have replaced $\int_0^\infty dx$ with

$$\int_0^\infty dx \frac{2}{\pi} \int_0^\infty dq \frac{\sin qx}{q} = \frac{2}{\pi} \int_0^\infty \frac{dq}{q^2}.$$

The result (40) is meaningful if $\nu(q \rightarrow 0) \rightarrow 1/\epsilon_\perp^{(m)}$, which we will show later is true. The remainder term may be written as

$$\begin{aligned}
RD_x(0) &= \int_{-a/2}^{a/2} dx \{ \Theta(-x)E_x(x) - \bar{\Theta}(-x)E_x^<(x) + [\Theta(x) - \bar{\Theta}(x)]E_x^>(x) \} \\
&= \int_{-a/2}^{a/2} dx \{ [\Theta(-x) - \bar{\Theta}(-x)]D_x(0) + [\Theta(x) - \bar{\Theta}(x)]E_x^>(x) \} \\
&= \int_{-a/2}^{a/2} dx \{ [\Theta(x) - \bar{\Theta}(x)][E_x^>(x) - D_x(0)] \} , \tag{41}
\end{aligned}$$

where $\Theta(x) = Lt_{a \rightarrow 0} \bar{\Theta}(x)$. The field difference in the last line has both constant and fluctuating parts, but when multiplied by the difference of Θ functions all parts integrate to zero. Hence the remainder term vanishes so

$$(1 - 1/\epsilon_{\perp}^{(m)})d_{\perp} = \frac{2}{\pi} \int_0^{\infty} \frac{dq}{q^2} [\nu(q) - 1/\epsilon_{\perp}^{(m)}] , \tag{42}$$

identical in form to the jellium result. Our derivation of (42) used a specific choice of origin, but in fact the functional form of (42) is independent of that choice.³⁶ The function $\nu(q)$ changes in a complicated way when the origin is translated by b , but as SC showed d_{\perp} merely shifts to $d_{\perp} - b$.

As a slight digression we note here for completeness the form of d_{\parallel} for our present model which only has crystallinity effects along the surface normal. The response to electric fields parallel to the surface is given by (local) free-electron formulas so d_{\parallel} is easily found. From SC the analog of (33) is

$$(1 - \epsilon_{\parallel}^{(m)})d_{\parallel} = \int_{-\infty}^{\infty} dx [D_{\parallel}(x) - \bar{D}_{\parallel}^0(x)]/E_{\parallel}(0) , \tag{43}$$

which reduces to the frequency-independent real-valued result

$$d_{\parallel} = \int_{-\infty}^{\infty} dx [\bar{\Theta}(x)n_{0,B}(x) - n_0(x)]/\bar{n}_{0,B} , \tag{44}$$

where $n_0(x)$ is the equilibrium density, $n_{0,B}(x)$ describes its variation in an infinite "crystal," and $\bar{n}_{0,B}$ is the average of $n_{0,B}(x)$ over a unit cell. The macroscopic dielectric function for fields parallel to the surface is

$$\epsilon_{\parallel}^{(m)} = 1 - \frac{4\pi\bar{n}_{0,B}e^2}{m\omega^2} , \tag{45}$$

and similar equations relate the D_{\parallel} 's in (43) to E_{\parallel} , which is nearly constant. An evaluation of (44) requires only the ground-state density profile, but represents merely a slight improvement over a full jellium model for which $n_{0,B}$ is constant.

C. Integral equation solution

Having shown via Eqs. (29), (31), (32), and (42) the utility of the function $\nu(q)$ we consider next its evaluation from (27). Again a drastic (but improvable) approximation will simplify the initial estimate. The susceptibility $\chi_0(q, q')$ has both smooth and singular contributions, with the latter coming solely from the bulk response of the system. Our approximation is to keep only the singular terms, which has an uncontrolled effect on the surface contributions. In a jellium calculation such an approximation yields the so-called semiclassical infinite barrier model, which has often been used but is now generally re-

garded as allowing only qualitative insights.¹⁻⁹ Our opinion is that any complete theory must evaluate both types of contribution to χ_0 , but one must start somewhere tractable.

The appearance of the singular terms is more involved in the presence of crystallinity effects than for jellium, since wave vectors are only conserved to within multiples of $g_0 = 2\pi/a$. We claim that χ_0 separates into³⁶

$$\begin{aligned}
\chi_0(q, q') &= \chi_{0,B}(q, q')\delta(k - k') \\
&\quad + \chi_{0,B}(q, -q')\delta(k + k' - g_0) + \bar{\chi}_0(q, q') , \tag{46}
\end{aligned}$$

where

$$q = k + g, \quad q' = k' + g' , \tag{47}$$

with $0 < k, k' < g_0$ and $g = ng_0, g' = n'g_0$ with n and n' non-negative integers. The $\chi_{0,B}(q, q')$ are Fourier transforms of the bulk susceptibility:

$$\begin{aligned}
\chi_{0,B}(k + ng_0, k + n'g_0) \\
&\equiv \chi_k(n, n') = \frac{1}{a} \int_0^a dx \int_{-\infty}^{\infty} dx' e^{-i(k + ng_0)x} \\
&\quad \times \chi_{0,B}(x, x') e^{i(k + n'g_0)x'} , \tag{48}
\end{aligned}$$

and the $\bar{\chi}_0$ function contains the nonsingular contributions that we ignore here. For a jellium model the g 's would not appear, which would remove the second singular term and make the first diagonal in the total wave vector, rather than diagonal only in the reduced wave vector. In this limit the SCIB solution for ν is trivial:

$$\nu_{\text{SCIB}}^{\text{jellium}}(q) = 1/\epsilon_B(q) , \tag{49}$$

where

$$\epsilon_B(q) = 1 - \chi_{0,B}(q, q')\nu(q) \tag{50}$$

is (in the RPA) the Lindhard bulk dielectric function. We used (49) and (50) to determine the jellium curves in Figs. 1 and 2.

The SCIB solution for ν when one keeps (one-dimensional) crystallinity effects is more involved. It is helpful to define a symmetrized bulk dielectric function matrix as

$$\begin{aligned}
\delta(k - k')\epsilon_B(q, q') \\
&\equiv \epsilon_k(n, n')\delta(k - k') \\
&= \delta(k - k')[\delta_{n, n'} - \nu^{1/2}(q)\chi_{0,B}(q, q')\nu^{1/2}(q')] , \tag{51}
\end{aligned}$$

where

$$\nu^{1/2}(q) = \frac{(4\pi e^2)^{1/2}}{k + ng_0} . \tag{52}$$

Then the combination of Eqs. (27) and (46) can be written as

$$\begin{aligned} & \sum_{n' \geq 0} \int_0^\infty dk' [v^{-1/2}(q)\epsilon_k(n, n')v^{1/2}(q')\delta(k-k') \\ & + v^{-1/2}(q)\epsilon_k(n, -n'-1) \\ & \times v^{1/2}(q')\delta(k+k'-g_0)]\nu(q') \\ & = 1 + \int_0^\infty d\bar{q} \bar{\chi}_0(q, \bar{q})v(\bar{q})\nu(\bar{q}) . \end{aligned} \quad (53)$$

We can make the second term on the left-hand side of (53) look like the first by some notational manipulation. After the integration over k' , replace in the second term n' with $-m-1$:

$$\begin{aligned} & \sum_{n' \geq 0} v^{-1/2}(q)\epsilon_B(q, -(g_0-k+n'g_0)) \\ & \times v^{1/2}(-(g_0-k+n'g_0))\nu(g_0-k+n'g_0) \\ & = \sum_{m < 0} v^{-1/2}(q)\epsilon_B(q, k+mg_0) \\ & \times v^{1/2}(k+mg_0)\nu(-(k+mg_0)) . \end{aligned} \quad (54)$$

Then (53) becomes

$$\begin{aligned} & \sum_{n'} v^{-1/2}(q)\epsilon_k(n, n')v^{1/2}(q')\nu(|q'|) \\ & = 1 + \int d\bar{q} \bar{\chi}_0(q, \bar{q})v(\bar{q})\nu(\bar{q}) \end{aligned} \quad (55)$$

where now $q'=k+n'g_0$ and the sum on n' runs over all integers. To make the left-hand side of (55) appear as a multiplication by a square matrix, consider the changes in (55) under the replacement $k \rightarrow g_0-k$. At the same time let $n \rightarrow -m-1$ with $m < 0$ and $n' \rightarrow -m'-1$ with m' unrestricted. Then

$$q \rightarrow (g_0-k) - (m+1)g_0 = -(k+mg_0) = |k+mg_0| \quad (56)$$

and

$$q' \rightarrow (g_0-k) - (m'+1)g_0 = -(k+m'g_0) . \quad (57)$$

Our assumption of an inversion symmetry in the bulk provides the relation

$$\begin{aligned} & v^{-1/2}(q)\epsilon_B(q, q')v^{1/2}(q') \\ & = v^{-1/2}(-q)\epsilon_B(-q, -q')v^{1/2}(-q') . \end{aligned} \quad (58)$$

Combining all these changes, (55) becomes

$$\begin{aligned} & \sum_{m'} v^{-1/2}(q)\epsilon_k(m, m')v^{1/2}(q')\nu(|q'|) \\ & = 1 + \int d\bar{q} \bar{\chi}_0(|q|, \bar{q})v(\bar{q})\nu(\bar{q}) , \end{aligned} \quad (59)$$

where now $q=k+mg_0$, $q'=k+m'g_0$, and m is a negative integer. Together (55) and (59) imply that

$$\sum_{n'} B_k(n, n')\nu(|q'|) = 1 + \int d\bar{q} \bar{\chi}_0(|q|, \bar{q})v(\bar{q})\nu(\bar{q}) , \quad (60)$$

where the square matrix $B_k(n, n')$ is defined by

$$B_k(n, n') = v^{-1/2}(q)\epsilon_k(n, n')v^{1/2}(q') , \quad (61)$$

with n and n' integers. The SCIB solution then appears as

$$\nu_{\text{SCIB}}(|q|) = \sum_{n'} B_k^{-1}(n, n') , \quad (62)$$

and the same matrix inverse would be needed for the general solution of (60).

D. Subtraction terms

As we show in Sec. III, the matrix in (61) is readily calculated. However, its inverse can fail to exist at particular values of q . Since our formulas for, say, η and d_\perp , require integrals over q , these singular points cause numerical difficulties. We shall treat them by the same methods used above the bulk plasmon threshold in jellium where the $\epsilon_B(q)$ of (50) has a single zero.^{34,37} This involves subtracting from the exact B_k^{-1} functions which reproduce its pole structure, but which are analytically tractable. Our symmetrized definition of $\bar{\epsilon}_k$ is especially useful in this task since it leads to

$$B_k^{-1}(n, n') = v^{-1/2}(q)\epsilon_k^{-1}(n, n')v^{1/2}(q') \quad (63)$$

in which the two sorts of poles that occur do so in separate factors, either $v^{1/2}(q')$ or $\epsilon_k^{-1}(n, n')$. We treat these in turn.

The singularities due to $v^{1/2}(q')$ are easy to locate and are always present. Since $q=k+ng_0$ and $q'=k+n'g_0$ we have when $q' \rightarrow 0$ that $q \rightarrow (n-n')g_0$. Hence near these singularities

$$\begin{aligned} B_k^{-1}(n, n') & = \frac{q}{q'} \epsilon_B^{-1}(q, q') \\ & \approx \frac{(n-n')g_0}{q - (n-n')g_0} \epsilon_B^{-1}((n-n')g_0, 0) . \end{aligned} \quad (64)$$

Summing over n' , as required by (62), we define

$$\begin{aligned} \nu^{(1)}(q) & = \sum_{n'} \frac{(n-n')g_0}{q - (n-n')g_0} \epsilon_B^{-1}((n-n')g_0, 0) \\ & = \sum_{(g \neq 0)} \frac{g}{q-g} \epsilon_B^{-1}(g, 0) \\ & = \sum_{g > 0} \frac{2g^2}{q^2 - g^2} \epsilon_0^{-1}(n, 0) , \end{aligned} \quad (65)$$

where the last step follows from the symmetry $\epsilon_B^{-1}(g, 0) = \epsilon_B^{-1}(-g, 0)$. We refer to the singular structures in (64) and (65) as zone-boundary singularities. They are responsible for the local-field oscillations evident in both Figs. 1 and 2. Their periods are independent of frequency and of the form a/n with n an integer, but their amplitudes depend on ω since the $\epsilon_0^{-1}(n, 0)$ do. When we need to integrate over q , the singular structures in (65) are treated as requiring principal value integrals. To illustrate we obtain for

$$\begin{aligned}
\left[\frac{1}{\epsilon_{\perp}^{(m)} - 1} \right] \eta^{(1)}(x) &= \frac{2}{\pi} \int_0^{\infty} dq \frac{\sin qx}{q} v^{(1)}(q) \\
&= \int_0^x dx' \frac{2}{\pi} \int_0^{\infty} dq \cos qx' v^{(1)}(q) \\
&= 2 \sum_{n>0} \epsilon_0^{-1}(n,0) (\cos ng_0 x - 1) \quad (66)
\end{aligned}$$

and for

$$\begin{aligned}
\left[1 - \frac{1}{\epsilon_{\perp}^{(m)}} \right] d_{\perp}^{(1)} &= \frac{2}{\pi} \int_0^{\infty} \frac{dq}{q^2} [v^{(1)}(q) - v^{(1)}(0)] \\
&= \sum_{g>0} \epsilon_0^{-1}(n,0) \frac{2}{\pi} \int_{-\infty}^{\infty} \frac{dq}{q^2 - g^2} = 0. \quad (67)
\end{aligned}$$

The standing-wave form of the fluctuating structure in (66) is what we expected to obtain, but (67) shows that its presence has no direct effect on d_{\perp} .

The other singularities in (63) arise from the divergences of $\vec{\epsilon}_k^{-1}(n, n')$, more specifically from the zeros of $\det(\vec{\epsilon}_k)$. Hence their location only depends on k , not on n or n' . If we write

$$\det(\vec{\epsilon}_k) = \frac{k - k_0}{R_0} + \mathcal{O}(k - k_0)^2, \quad (68)$$

then the values of k_0 and R_0 must be found numerically. The functional relation between k_0 and ω defines the dispersion relation of these so-called zone-boundary collective states (ZBCS's).^{20-22,38} Since they are excitations of the bulk, (68) also implies that

$$\det(\vec{\epsilon}_k) = \frac{k - (g_0 - k_0)}{(-R_0)} + \mathcal{O}(k - (g_0 - k_0))^2; \quad (69)$$

i.e., the poles always appear in ‘‘conjugate’’ pairs. To approximate $\vec{\mathbf{B}}_k^{-1}$ near them we recall that the inverse of a matrix can be expressed as

$$B_k^{-1}(n, n') = N(q, q') / \det(\vec{\mathbf{B}}_k), \quad (70)$$

where $\vec{\mathbf{N}}_k$ is the classical adjoint matrix.³⁹ Then for k near k_0 or $g_0 - k_0$

$$\begin{aligned}
B_k^{-1}(n, n') &\equiv \sum_l R_0 \left[\frac{N_{k_0}(l, n')}{q - (k_0 + lg_0)} \right. \\
&\quad \left. - \frac{N_{g_0 - k_0}(l, n')}{q - (g_0 - k_0 + lg_0)} \right]. \quad (71)
\end{aligned}$$

Since $\vec{\mathbf{N}}_k$ has the same symmetries as $\vec{\mathbf{B}}_k$, see (58),

$$\begin{aligned}
N_{g_0 - k_0}(l, n') &= N(g_0 - k_0 + lg_0, g_0 - k_0 + n'g_0) \\
&= N(k_0 + mg_0, k_0 + m'g_0) = N_{k_0}(m, m'), \quad (72)
\end{aligned}$$

where $m = -(l + 1)$ and $m' = -(n' + 1)$. Then if we sum (71) over n' to define $v^{(2)}(q)$, it can be reduced to

$$\begin{aligned}
v^{(2)}(q) &= R_0 \sum_{m, m'} N_{k_0}(m, m') \left[\frac{1}{q - (k_0 + mg_0)} \right. \\
&\quad \left. - \frac{1}{q + (k_0 + mg_0)} \right] \\
&= R_0 \sum_m \frac{2(k_0 + mg_0)}{q^2 - (k_0 + mg_0)^2} M_{k_0}(m), \quad (73)
\end{aligned}$$

where

$$M_{k_0}(m) = \sum_{m'} N_{k_0}(m, m'). \quad (74)$$

To make the subtraction function (73) appear similar to that in the jellium model³⁴ we further define

$$\gamma_m = \frac{2R_0 M_{k_0}(m)}{(1/\epsilon_{\perp}^{(m)} - 1)(k_0 + mg_0)}, \quad (75)$$

so

$$v^{(2)}(q) = (1/\epsilon_{\perp}^{(m)} - 1) \sum_m \frac{\gamma_m (k_0 + mg_0)^2}{q^2 - (k_0 + mg_0)^2}. \quad (76)$$

The singularities here are treated in integrals by replacing $k_0 \rightarrow k_0 + i0^+$ to represent the creation of a ZBCS propagating away from the surface. This yields for

$$\left[\frac{1}{\epsilon_{\perp}^{(m)} - 1} \right] \eta^{(2)}(x) = \frac{2}{\pi} \int_0^{\infty} dq \frac{\sin qx}{q} v^{(2)}(q) \quad (77)$$

the simple result

$$\eta^{(2)}(x) = \sum_m \gamma_m (e^{i(k_0 + mg_0)x} - 1), \quad (78)$$

and for

$$\left[1 - \frac{1}{\epsilon_{\perp}^{(m)}} \right] d_{\perp}^{(2)} = \frac{2}{\pi} \int_0^{\infty} \frac{dq}{q^2} [v^{(2)}(q) - v^{(2)}(0)] \quad (79)$$

the finite contribution

$$d_{\perp}^{(2)} = \sum_m \frac{\gamma_m}{i(k_0 + mg_0)}. \quad (80)$$

To complete the evaluation of η and d_{\perp} for the SCIB approximation is now a well-defined numerical task. One writes

$$v_{\text{SCIB}}(q) = \bar{v}(q) + v^{(1)}(q) + v^{(2)}(q), \quad (81)$$

where \bar{v} is determined by substituting from (62), (65), and (76). By construction, $\bar{v}(q)$ has no singular structures. This makes all required integrals well behaved if we note the following limiting values. As $q \rightarrow \infty$, $v^{(1)}$ and $v^{(2)}$ vanish while v_{SCIB} and \bar{v} tend to 1. As $q \rightarrow 0$,

$$\begin{aligned}
v_{\text{SCIB}}(q) &= \sum_{n'} \frac{q}{q - (n - n')g_0} \epsilon_k^{-1}(n, n') \\
&\rightarrow \sum_{n'} \frac{k}{k + n'g_0} \epsilon_k^{-1}(0, n') \\
&= \epsilon_0^{-1}(0, 0) + O(q^2) \\
&\equiv 1/\epsilon_{\perp}^{(m)}. \tag{82}
\end{aligned}$$

The identification in the last line of (82) is the appropriate version for our anisotropic system of the well-known connection between microscopic and macroscopic ϵ 's.^{26,40-42} For us it ensures that the integral (42) for d_{\perp} is convergent. The limiting values of the $v^{(i)}$ are

$$v^{(1)}(q \rightarrow 0) \rightarrow -2 \sum_{n>0} \epsilon_0^{-1}(n, 0) + O(q^2), \tag{83}$$

$$v^{(2)}(q \rightarrow 0) \rightarrow (1 - 1/\epsilon_{\perp}^{(m)}) \sum_m \gamma_m + O(q^2). \tag{84}$$

From (82)–(84) the limiting behavior of \bar{v} immediately follows. To make contact with jellium results define

$$\bar{S}(q) = \bar{v}(q) - 1 - 2 \sum_{n>0} \epsilon_0^{-1}(n, 0). \tag{85}$$

Then

$$d_{\perp} = \sum_m \frac{-i\gamma_m}{k_0 + mg_0} + \frac{2}{\pi} \int_0^{\infty} \frac{dq}{q^2} \left[1 + \sum_m \gamma_m + \frac{\bar{S}(q)}{1 - 1/\epsilon_{\perp}^{(m)}} \right], \tag{86}$$

where

$$\bar{S}(q \rightarrow 0) = - \left[1 - \frac{1}{\epsilon_{\perp}^{(m)}} \right] \left[1 + \sum_m \gamma_m \right] + O(q^2), \tag{87}$$

which compares directly with Eq. (21) in Ref. 34.

To end this section we remark that we have formulated the subtractions from \bar{B}_k^{-1} so the results would still apply if $\bar{\chi}_0$ were retained. The same general scheme could also be used when three-dimensional lattice structure is allowed.

III. MODEL CALCULATION

To illustrate the formalism we now describe a pseudopotential evaluation of the basic formulas. The parameters are chosen to model the (110) face of Li since this system has relatively strong lattice scattering and shows significant deviations from jellium predictions. The lattice constant along the surface normal is $a = 2.48 \text{ \AA}$ so $g_0 = 2\pi/a = 2.54 \text{ \AA}^{-1}$. With one conduction electron per atom the jellium $r_s = 3.26a_0$, where a_0 is the Bohr radius. The lattice potential energy is described by a single Fourier component pseudopotential

$$V(x) = 2V_0 \cos(g_0 x) \tag{88}$$

whose strength is $V_0 = 1.44 \text{ eV}$. This choice, plus the assumption of an isotropic effective mass $m^*/m = 1.09$, allows a reasonable representation of the band dispersion at low energy in the (110) direction.^{21,22,43,44} Our treatment is similar in spirit, but different in detail, from the two-

band model used by Sturm and Oliveira. Although both models allow just one Fourier component in $V(x)$, our band structure is explicitly periodic in an extended zone scheme. This is necessary since we eventually need integrals over q of the response function. For the same reason we also keep all local-field effects. Finally, we note that although we are using a pseudopotential for the lattice scattering, we do not try to correct for the difference between pseudocharge densities and true charge densities.

A picture of the (one-dimensional) band structure is shown in Fig. 3. The first Brillouin zone has been chosen so the reduced wave vector remains positive, as is appropriate for the cosine Fourier transforms of our formalism. The Fermi energy is determined by requiring that the average bulk density be given by $3/(4\pi r_s^3 a_0^3)$; its value is $\epsilon_F = 4.04 \text{ eV}$, slightly smaller than the jellium result $\epsilon_F^0 = 4.33 \text{ eV}$. The Fermi wave vector $p_F = 1.20 \text{ \AA}^{-1}$ is larger than p_F^0 , but a bit smaller than $g_0/2 = 1.27 \text{ \AA}^{-1}$.

The bulk susceptibility defined in (48) is calculated from

$$\begin{aligned}
\chi_{0,B}(x, x') &= \frac{2}{A} \sum_{p,p'} \sum_{l,l'} \sum_{\mathbf{P}} \frac{f_{pl,\mathbf{P}} - f_{p'l',\mathbf{P}}}{\epsilon_{pl} + \hbar\omega - \epsilon_{p'l'} + i0^+} \\
&\quad \times \psi_{pl}^*(x) \psi_{p'l'}(x) \psi_{p'l'}^*(x') \psi_{pl}(x'), \tag{89}
\end{aligned}$$

where p and p' label wave vectors in the first zone, l and l' are band indices, \mathbf{P} is the common wave vector parallel to the surface, and the overall factor of 2 is for spin. The f 's are Fermi occupation factors and will be evaluated at zero temperature. Their argument is the total energy of an electron state, whereas only the difference of "normal" energies survives in the denominator. The wave functions are also one dimensional (Bloch waves). The plane wave variation in \mathbf{X} has been Fourier transformed away.

In Fig. 4 we compare the continua of single-particle bulk excitations for our band-structure model and its jell-

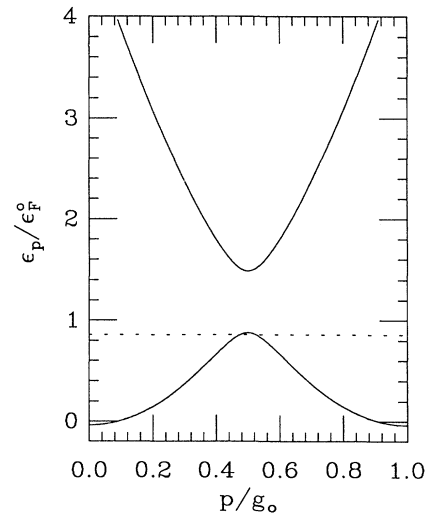


FIG. 3. Band structure along the (110) direction in Li. The solid curves give the electron energy ϵ_p vs (reduced) wave vector p . The dashed horizontal line is the Fermi level.

lium limit, when $V_0 \rightarrow 0$ and $m^* \rightarrow m$. The bounded regions are where the imaginary part of $\chi_{0,B}(x, x')$ [and also of $\epsilon_B(q, q')$] is nonzero. The gap separating intraband from interband excitations is a direct consequence of lattice scattering. We also show in Fig. 4 the dispersion of undamped bulk collective modes. These curves are determined by requiring $\det|\vec{\epsilon}_k| = 0$. For the jellium model the only mode that appears is the bulk plasmon, while the band-structure effects lead to a damping of this mode due to interband transitions and the appearance of

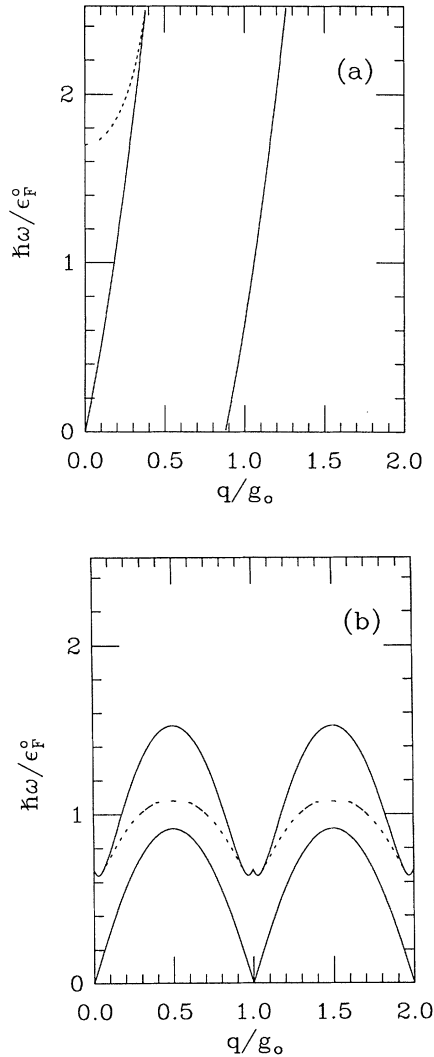


FIG. 4. Comparison of electron-hole pair continuum of excitation for (a) the jellium model and (b) the Li(110) band-structure model. The solid curves are the boundaries in frequency-wave-vector space between regions of zero and finite excitation probability. In (a) the excitations occur between the curves while in (b) the excitations are either below the lower solid curve (intraband) or above the upper solid curve (interband). The structure in (b) is periodic in the wave vector q . The dashed curves describe the dispersion of undamped collective modes. In (a) the bulk plasmon exists up to $\hbar\omega/\epsilon_F^0 = 2.52$. In (b) the ZBCS begins and ends away from the zone boundaries at $q = 0$ and g_0 .

a new collective mode in the continuum gap, the ZBCS.

We next show several views of the dielectric matrix⁴¹ by plotting its values along certain cuts through Fig. 4. The macroscopic limit, defined by (82), is given in Fig. 5. The real part of $\epsilon_1^{(m)}$ is slightly changed from the jellium limit, but the interband absorption makes the imaginary part nonzero above a threshold.

In Fig. 6 we compare several fixed frequency plots of $\epsilon_k(0, 0)$. At $\hbar\omega/\epsilon_F^0 = 0.5$, one is below the interband threshold so the band structure and jellium pictures are fairly similar. At $\hbar\omega/\epsilon_F^0 = 0.9$ there are considerable differences. Notice in particular the extra zeros of $\epsilon_k(0, 0)$. They occur close to the k_0 and $g_0 - k_0$ values of the ZBCS since local-field effects—specifically the difference between $\epsilon_k(0, 0)$ and $\det|\vec{\epsilon}_k|$ —are not large at this frequency. Finally, at $\hbar\omega/\epsilon_F^0 = 2.0$ one is in the plasmon range for jellium, but there is no complete zero for the band-structure case.

In Fig. 7 we compare the d_1 's. For the band-structure case, reciprocal-lattice vectors out to $\pm 4g_0$ were kept. There is clearly additional structure that begins sharply at the interband threshold and continues through and beyond the ZBCS band. We have separately plotted the direct contribution of the ZBCS to d_1 . It begins and ends with vanishing strength, just as in electron-loss spectra.^{21,22} Note that the imaginary part of d_1 changes sign below the bulk plasmon. In the presence of band structure the imaginary part of d_1 is not a direct measure of the absorption.⁴ We have also done analogous calculations for Na, whose pseudopotential strength is an order of magnitude smaller than that of Li. The deviations between the Na results and a jellium limit are almost indiscernible since effects on d_1 scale roughly with V_0^2 .

Returning to Fig. 7 it is interesting to notice that the interband scattering is strong enough to significantly round off the plasmon divergence that appears in the jellium d_1 . We emphasize that this lifetime broadening is being calculated microscopically here, not fudged by an *ad*

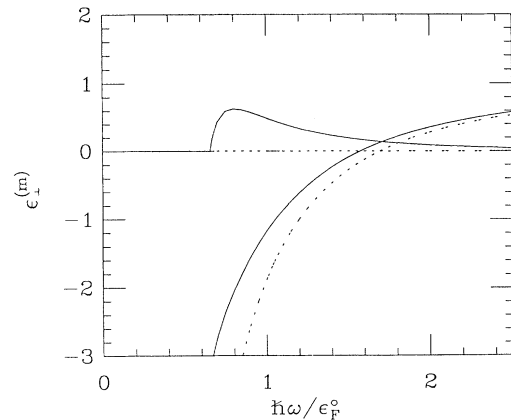


FIG. 5. Macroscopic dielectric function vs frequency for response along the surface normal. Both the real and imaginary parts of $\epsilon_1^{(m)}$ are drawn with solid lines. The dashed curves give the jellium result; note that its imaginary part is identically zero.

hoc parameter. The appearance of the field when the damped plasmon is present is shown in Fig. 8, which like Figs. 1 and 2 is determined from (32) with ν replaced by $\bar{\nu} + \nu^{(1)} + \nu^{(2)}$. The plasmon oscillation is evident, but it decays as one moves into the bulk. In Fourier space there is a (rounded) polelike structure in the $\bar{\epsilon}_k^{-1}$ versus k curves which we can handle numerically without subtrac-

tions. However, the neglect of zone planes other than (110) is a serious omission in this higher-frequency range.^{21,22}

To sum up, we would describe our results as a promising beginning on a difficult problem. The derivation in Sec. II has shown how to reduce a formal prescription²⁸ to a practical evaluation scheme. Several severe approxi-

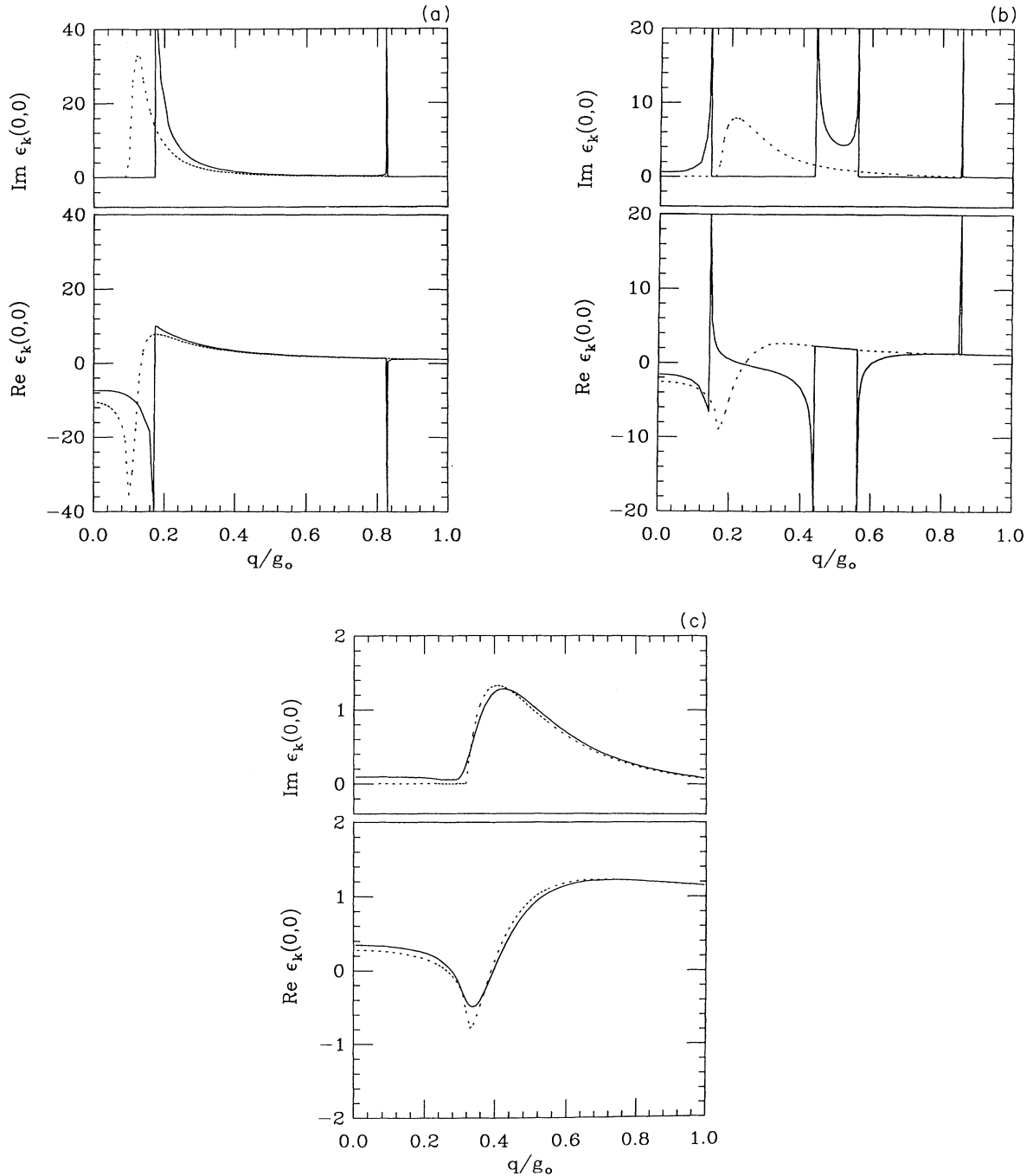


FIG. 6. Comparison of microscopic dielectric functions. In each panel both the real and imaginary (bottom and top) parts of $\epsilon_k(0,0)$ are plotted for both the band-structure and jellium (solid and dashed) models. The fixed frequency is (a) $0.5\epsilon_F^0$, (b) $0.9\epsilon_F^0$, and (c) $2.0\epsilon_F^0$. The singularities that go off scale are inverse square-root divergences.

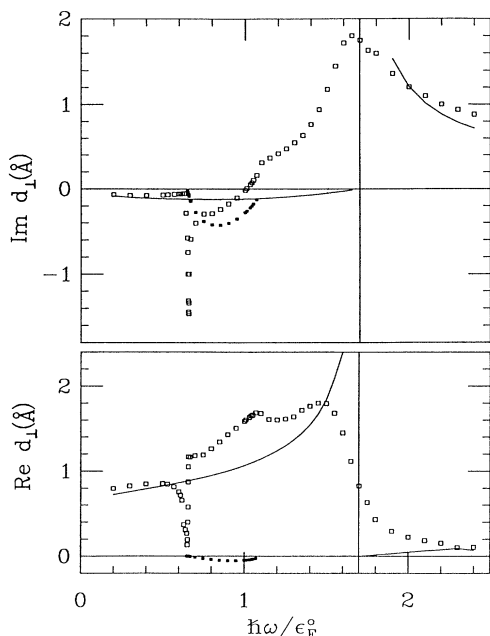


FIG. 7. Comparison of d_1 for the band-structure (open squares) and jellium (solid line) models. The real and imaginary parts of d_1 are plotted separately. The solid squares give the direct contribution (80) of the ZBCS over the frequency range where it exists as an undamped mode.

mations were made in this first effort, but there appears to be no fundamental impediment to their removal. We can envision the retention of $\bar{\chi}_0$, starting first with an infinite barrier model³⁶ and then progressing to finite and self-consistently determined barriers. Also, an analysis that accounts for crystallinity effects in three dimensions should be a feasible, but considerable challenge. One can go beyond a RPA description of many-body effects too, incorporating, say, a time-dependent local-density-functional scheme. Our confidence in the possibility of this succession of improvements rests on the facts that a similar path was followed for the jellium models¹⁻¹¹ and that the formal developments here show that crystallinity

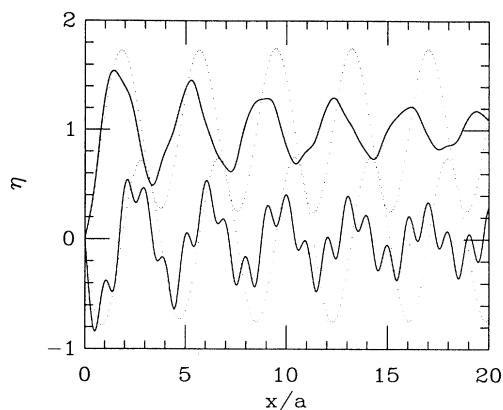


FIG. 8. Same as Fig. 1 except the frequency of the external perturbation is here $2.0\epsilon_F^0$. The local-field oscillations, which in contrast to Fig. 1 are now more evident in the imaginary part of η , still have period a .

effects do not change the basic structure of the theory. The awareness of this possibility plus the existence of relevant experimental data¹³⁻¹⁸ will hopefully lead to steady improvements. Although the present numerical results cannot be directly compared with experiment, they do give first measures of the existence and importance of effects totally absent in jellium models. Their evaluation has also provided a calculational basis onto which one can build systematic refinements. We look forward to this continuing progress.

ACKNOWLEDGMENTS

We wish to thank Dr. Wei Chen for help at the beginning of this work. We are also grateful to Dr. K. Sturm and Dr. L. E. Oliveira for useful discussions of their work. This effort was supported in part by the National Science Foundation through Grant No. DMR-89-03851. Some of the calculations were done on the Cray Research, Inc. X-MP/48 system at the National Center for Supercomputing Applications at the University of Illinois at Urbana-Champaign (Champaign, IL).

¹K. L. Kliewer, *Surf. Sci.* **101**, 80 (1980).

²P. Apell, *Phys. Scr.* **24**, 795 (1981).

³B. B. Dasgupta and D. E. Beck, in *Electromagnetic Surface Modes*, edited by A. D. Boardman (Wiley, London, 1982), p. 77.

⁴P. J. Feibelman, *Prog. Surf. Sci.* **12**, 287 (1982).

⁵P. Apell, A. Lyungbert, and S. Lundqvist, *Phys. Scr.* **30**, 367 (1984).

⁶A. M. Brodsky and M. I. Urbakh, *Prog. Surf. Sci.* **15**, 121 (1984).

⁷G. W. Ford and W. H. Weber, *Phys. Rep.* **113**, 195 (1984).

⁸F. Forstmann and R. R. Gerhardt, *Metal Optics Near the Plasma Frequency* (Springer, Berlin, 1986).

⁹W. L. Schaich and K. Kempa, *Phys. Scr.* **35**, 204 (1987).

¹⁰A. Liebsch, *Phys. Scr.* **35**, 354 (1987).

¹¹A. G. Eguiluz, *Phys. Scr.* **36**, 651 (1987).

¹²K. Kempa, A. Liebsch, and W. L. Schaich, *Phys. Rev. B* **38**, 12 645 (1988).

¹³K.-D. Tsuei, E. W. Plummer, and P. J. Feibelman, *Phys. Rev. Lett.* **63**, 2256 (1989).

¹⁴S. Suto, K.-D. Tsuei, E. W. Plummer, and E. Burstein, *Phys. Rev. Lett.* **63**, 2590 (1989).

¹⁵K.-D. Tsuei, E. W. Plummer, A. Liebsch, K. Kempa, and P. Bakshi, *Phys. Rev. Lett.* **64**, 44 (1990).

¹⁶M. Rocca and U. Valbusa, *Phys. Rev. Lett.* **64**, 2398 (1990).

¹⁷A. Liebsch, G. Hincelin, and T. López-Riós, *Phys. Rev. B* **41**, 10 463 (1990).

¹⁸M. Rocca, F. Biggio, and U. Valbusa, *Phys. Rev. B* **42**, 2835 (1990).

¹⁹J. D. Jackson, *Classical Electrodynamics* (Wiley, New York, 1975).

²⁰K. Sturm and L. E. Oliveira, *Phys. Rev. B* **30**, 4351 (1984).

- ²¹K. Sturm and L. E. Oliveira, *Europhys. Lett.* **9**, 257 (1989).
²²K. Sturm and L. E. Oliveira, *Phys. Rev. B* **40**, 3672 (1989).
²³R. Del Sole, *Solid State Commun.* **37**, 537 (1981).
²⁴W. L. Mochan, R. Fuchs, and R. G. Barrera, *Phys. Rev. B* **37**, 771 (1983).
²⁵R. Del Sole and E. Fiorino, *Phys. Rev. B* **29**, 4631 (1984).
²⁶W. L. Mochan and R. G. Barrera, *Phys. Rev. B* **32**, 4984 (1985); **32**, 4989 (1985).
²⁷A. Muramatsu and W. Hanke, in *Structure and Dynamics of Surfaces II*, Vol. 43 of *Topics in Current Physics*, edited by W. Schommers and P. von Blanckenhagen (Springer, New York, 1987).
²⁸W. L. Schaich and W. Chen, *Phys. Rev. B* **39**, 10 714 (1989).
²⁹F. Manghi, R. Del Sole, A. Selloni, and E. Molinari, *Phys. Rev. B* **41**, 9935 (1990).
³⁰Y.-C. Chang and D. E. Aspnes, *Phys. Rev. B* **41**, 12 002 (1990).
³¹W. Chen and W. L. Schaich, *Surf. Sci.* **218**, 580 (1989).
³²K. Kempa and W. L. Schaich, *Phys. Rev. B* **34**, 547 (1986).
³³K. Kempa and W. L. Schaich, *Phys. Rev. B* **37**, 6711 (1988).
³⁴K. Kempa and W. L. Schaich, *Phys. Rev. B* **39**, 13 139 (1989).
³⁵D. E. Beck and B. B. Dasgupta, *Phys. Rev. B* **12**, 1995 (1975).
³⁶J.-T. Lee and W. L. Schaich (unpublished).
³⁷R. R. Gerhardts and K. Kempa, *Phys. Rev. B* **30**, 5704 (1984).
³⁸E.-Ni Foo and J. J. Hopfield, *Phys. Rev.* **173**, 635 (1968).
³⁹P. C. Shields, *Linear Algebra* (Addison-Wesley, Reading, MA, 1964).
⁴⁰S. L. Adler, *Phys. Rev.* **126**, 413 (1962).
⁴¹N. Wisser, *Phys. Rev.* **129**, 62 (1963).
⁴²D. L. Johnson, *Phys. Rev. B* **9**, 4475 (1975); **12**, 3428 (1975).
⁴³W. Y. Ching and J. Callaway, *Phys. Rev. B* **9**, 5115 (1974).
⁴⁴H. Bross and G. Bohn, *Z. Phys. B* **20**, 261 (1975).